*SF2A 2006*
*D. Barret, F. Casoli, T. Contini, G. Lagache, A. Lecavelier, and L. Pagani (eds)*

# LINE FORMATION IN 3D RADIATION HYDRODYNAMICS SIMULATIONS OF RED SUPERGIANTS

A. Chiavassa[1], B. Plez[1], E. Josselin[1] and B. Freytag[2]

**Abstract.** We developed a 3D radiative transfer code which computes emerging spectra and monochromatic maps from radiative-hydrodynamic (RHD) simulations of red supergiant stars.
Computed emerging spectra show that our RHD models qualitatively reproduce the velocity amplitude and line asymmetries in observations. However, they cannot reproduce strong and weak lines simultaneously. This is explained by the shallow thermal gradient which weakens the contrast between strong and weak lines. The non-grey treatment of opacity in RHD models is planned in the near future to solve this problem.
Moreover, we are now studying the possibility to detect and measure the granulation pattern with interferometers such as VLTI/AMBER, using our monochromatic intensity maps and visibility calculations.

## 1 Introduction

Red supergiants (RSG) are evolved and massive (10-40$M_{\odot}$) stars. RSGs are influenced by a strong mass loss process of unknown origin. Shock waves associated with convective motions could drive the mass loss flows.
On-going 3D radiative hydrodynamics simulations of these stars, performed by Freytag et al. (2002) with the CO5BOLD code show a peculiar convection pattern, with giant cells evolving on a timescale of about one month.
We performed 3D pure LTE radiative transfer code in snapshots of 3D hydrodynamical simulation and we present here the results obtained in terms of spectral synthesis and intensity maps.

## 2 The radiative hydrodynamic simulation

The numerical simulations analyzed here are performed with "CO5BOLD" ("COnservative COde for the COmputation of COmpressible COnvection in a BOx of L Dimensions, l=2,3") developed by Freytag, Steffen, Ludwig and collaborators (see Freytag et al. 2002). Our simulations employ the *global star-in-a-box* setup: the computational domain is a cube with an equidistant grid in all directions. The radiation field treatment in the hydrodynamical simulations is strictly LTE and grey, and the opacity is a Rosseland mean, function of pressure and temperature. The necessary values are found by interpolation in a 2D table which has been merged at around 12 000 K from high-temperature OPAL data (Iglesias et al. 1992) and low-temperature PHOENIX data (Hauschildt et al. 1997) by Hans-Günter Ludwig. More technical informations can be found in the CO5BOLD Online User Manual (Freytag et al. 2004).
Our best model obtained so far has a solar composition, a resolution of $315^3$ grid points, a mass = $12M_{\odot}$, a stellar luminosity = $86300L_{\odot}$, an effective temperature of 3378K, $\log g = -0.37$ and a stellar radius = $860R_{\odot}$ (defined as the radius where $L/(4\pi R^2) = \sigma T^4$, i.e. where the local temperature is equal to the effective temperature).

[1] GRAAL, cc072, Université Montpellier II, F-34095 Montpellier cedex 05, France
[2] Los Alamos National Laboratory/Depart. of Physics and Astron. at Michigan State University, USA and Dept. for Astronomy and Space Physics at Uppsala University, Box 515, SE-751 20 Uppsala, Sweden

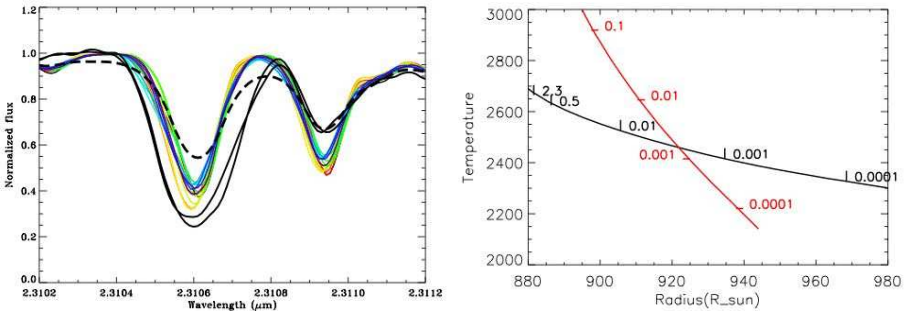


**Fig. 1.** *Left panel* : The time sequence computed for the high resolution model at 3378K, $\log g = -0.37$, $12M_{\odot}$ (each color refers to a snapshot with a step of 23 days) is compared to $\alpha$ Ori observations published by Wallace & Hinkle, 1996 (solid black line) around $2.3\mu m$ (CO lines). Neither 1D hydrostatic model exponentially convolved at 13km/s (dashed line) nor RHD model can reproduce strong and weak lines simultaneously. However, the RHD model does not require any extra macrotubulence to explain the line width. *Right panel* : Temperature profile averaged over time and spherical shells for the 3D hydrodynamical model described above (black line) and temperature profile of a 1D hydrostatic MARCS model (Plez, 1992) in red line. $\tau_{Rosseland}$ scales are indicated, they do not correspond because the black profile is a mean profile. In the outer atmosphere, the thermal gradient seems too low in the RHD model.

## 3 A posteriori radiation transfer in the hydrodynamical simulations

Radiation transfer is calculated along each ray in the RHD computational domain. The emerging intensity at the top of one ray of the box is computed by summing the contribution to the source function at different depths, taking into account Doppler shift caused by convective motions.
To speed up the calculations, extinction coefficients per unit mass are pre-tabulated as a function of temperature, density and wavelength with a resolution of 0.01 Å. We checked that this resolution is sufficient to ensure an accurate characterization of line profiles even after interpolation at the Doppler shifted wavelengths.

## 4 Results

### *4.1 Model thermal structure*

The radiation transport in CO5BOLD is characterized by a grey opacity treatment. The Rosseland mean gives higher weight to frequency regions with low opacities where, therefore, the greatest amount of radiation will be transported, while the weight of frequencies with high opacities are understimated. The Rosseland grey approximation is valid only in the deepest atmospheric layers at great optical depth. Figure 1 shows the comparison between the temperature profile of the RHD model averaged over time and over spherical shells, and the temperature profile of a 1D hydrostatic MARCS model (Plez 1992). Since the radius is defined differently in MARCS models (i.e., where $\tau_{Rosseland} = 1$) and RHD models (see above). We calculated 1D model effective radius following the RHD model procedure. The resulting effective temperature at this new radius is 3367K (instead of 3378K). In the outer atmosphere ($R > 920R_{\odot}$, $\tau_{Rosseland} \leq 0.001$), the 1D model appears cooler because of the detailed line blanketing calculation. The thermal gradient seems too low in the RHD model.

### *4.2 Spectral Synthesis*

We produced a time sequence, with a time-step of about 23 days covering 1.47 stellar years, of spectra computed with our best model described in Sect.2 : Figure 2 shows the calculations for two spectral regions. The velocity in the model differ by up to $\sim$ 15km/s across the atmosphere, in agreement to what Josselin & Plez (2006) found in their observations (between $\sim$ 5km/s and $\sim$ 17km/s). In order to study the depth-dependent phenomena in stellar atmosphere, the determination of the depth of formation of spectral line is required. For this purpose, we have computed the contribution function (CF) of different layers to a spectral line flux depression (see Magain 1986) and we considered the center of the line for each snapshot. In Fig.3 we examine two specific wavelengths: the pseudo-continuum corresponding to the wavelength 6162.13Å and the "very" strong line FeI at 5269.54Å (see Fig.2). We weighted the velocity field with CF to show at which velocity in the atmosphere

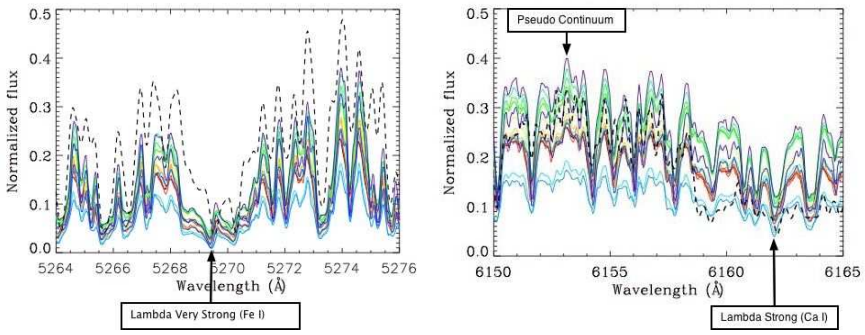


**Fig. 2.** Spectral synthesis computed for the model described in the text (color lines). The dashed line is a 1D hydrostatic model. We considered the center of the line to calculate contribution function to the spectral line depression.

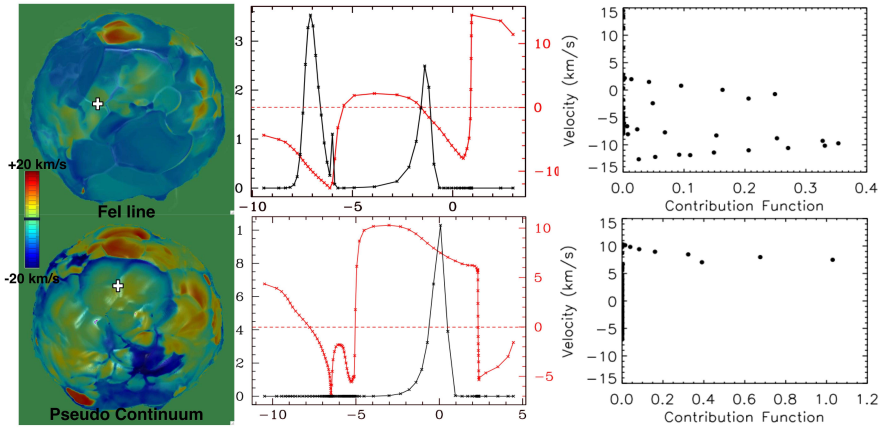


**Fig. 3.** First column displays the velocity field weighted with the contribution function (CF) to the line depression for two layers at different depth (colors follows usual radial convention), and for one snapshot : the "very" strong line of FeI (first row) and the pseudo continuum corresponding to 6162.13Å (second row). We selected two spots on the stellar surface (white crosses) and we calculated CF, second column shows CF versus the optical depth (black line) with the velocity overplotted (red line). Third column shows another representation of CF versus velocity.

the line forms (Fig.3). The contribution to the pseudo-continuum comes from layers falling inward with a velocity of $\sim +7$km/s (right hand panel), while the FeI line has its contribution from outgoing layers from a first velocity peak of $\sim -10$km/s and a second of $\sim -1$km/s. This double peak could cause the asymmetry in the observed cross correlation profiles (Josselin & Plez 2006). Furthermore, we compared two observations of $\alpha$ Ori (Wallace & Hinkle 1996) to our best RHD model in the infrared, where atomic lines are less blended than in the visible. As seen in Fig.1, the line centers span values between $-2$ and $+2$ km/s with respect to the hydrostatic model, and during short temporal sequences the lines become asymmetric. Our RHD model cannot reproduce strong and weak lines simultaneously, but it approximately reproduces the line width without the need for an extra macroturbulence (which is needed in the 1D model, that in addition does not reproduce the strong line). The RHD thermal gradient seems too low (see above) and the contrast between strong and weak lines is low. This explains why the RHD model cannot fully adjust the observations. Resolving this problem is a priority to get more reliable spectra. The non-grey treatment of opacity (through opacity binning) in CO5BOLD must be applied, even if it is extremely costly in terms of CPU time and the number of bins must be kept small. Moreover, since observed line profiles are time variable, RHD models represent an improvement with respect to hydrostatic models. Additionally, the model used here has not the right effective temperature (it is colder compared to $\alpha$ Ori effective temperature of 3650K, Levesque et al. 2005) and thus improvement in the comparison could be obtained with a warmer effective temperature in RHD models.

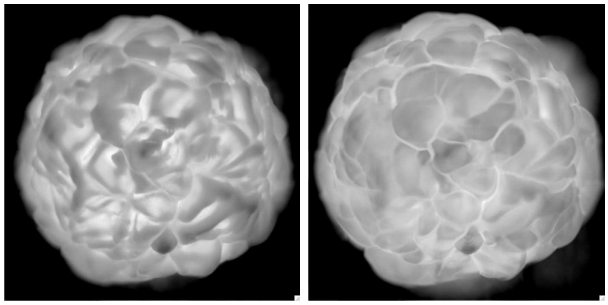

**Fig. 4.** Logarithmic maps of monochromatic intensity. Left panel shows to a pseudo continuum corresponding to 6162.13Å, while right panel displays the spectral line CaI at 6162.173Å. A grey scale is used and lighter shades correspond to higher intensities.

### *4.3 Intensity maps*

We computed maps of monochromatic intensity. Two examples are displayed in Fig.4 at wavelength corresponding to the CaI line and a nearby pseudo continuum (see Fig.2). These two wavelengths probe different depths in the stellar atmosphere. The brightest areas denote the maximum of intensity and structures are visible in both wavelengths. The granulation pattern seems more sharply defined in the line depression than in the pseudo-continuum. We are now studying the possibility to detect and measure the granulation pattern with the VLTI/AMBER, using such maps and visibility calculations.

## 5 Conclusions

The validation of our RSG RHD model with observations is now possible with our post processing analysis. We found that continuum and spectral line intensity maps show different structures. We plan to calculate visibility functions in the infrared to detect granulation with interferometers such as VLTI/AMBER. Another point is the RHD models improvement. The RHD models limits are : (1) The effective temperature is too low compared to prototypical RSG, we are now working on a set of new models with the same mass and resolution but with an higher effective temperatures. This analysis will help us find how velocity and flux fluctuations depend on RHD model effective temperature.(2) The radiation field treatment in RHD is not appropriate. The non-grey treatment of opacity should greatly improve the simulations in the atmospheric optically thin layers. (3) The resolution may not be sufficient, increasing the grid points up to $500^3$ will probably decrease flux fluctuations and it may show even smaller scale convective structures within the large scale granules already visible in lower resolution simulations (Fig.10 in Chiavassa et al. 2005).

We thank the "Centre Informatique National de l'Enseignement Supérieur" (CINES) for providing us with the computational resources required for part of this work.

## References

Chiavassa, A., Plez, B., Josselin, E., & Freytag, B. 2006, EAS Publications Series, 18, 177

Freytag, B., Steffen, M., & Dorch, B. 2002, Astronomische Nachrichten, 323, 213

Freytag, B., Steffen, M., Wedemeyer, S., & Ludwig, H.-G. 2004, CO5BOLD User Manual, http://www.astro.uu.se/∼bf/co5bold_main.html

Hauschildt, P. H., Baron, E., & Allard, F. 1997, ApJ, 483, 390

Iglesias, C. A., Rogers, F. J., & Wilson, B. G. 1992, ApJ, 397, 717

Josselin E., Plez B. 2006, submitted to A&A

Levesque, E. M., Massey, P., Olsen, K. A. G., Plez, B., Josselin, E., Maeder, A., & Meynet, G. 2005, ApJ, 628, 973

Magain, P. 1986, A&A, 163, 135

Plez, B. 1992, A&ASP, 94, 527

Schwarzschild, M. 1975, ApJ, 195, 137

Wallace, L., & Hinkle, K. 1996, ApJS, 107, 312